Dalton Transactions

PM-IRRAS and DFT investigation of the surface orientation of new Ir piano-stool complexes attached to Au (111)

Journal:	*Dalton Transactions*
Manuscript ID	DT-ART-08-2022-002730.R1
Article Type:	Paper
Date Submitted by the Author:	08-Oct-2022
Complete List of Authors:	Kubiak, Clifford; University of California San Diego, Department of Chemistry and Biochemistry Miller, Christopher; University of California San Diego, Chemistry and Biochemistry Brunner, Felix; University of California San Diego, Department of Chemistry and Biochemistry Kelly, H. Ray; Yale University Cheung, Po Ling; University of California San Diego, Department of Chemistry and Biochemistry Torquato, Nicole; University of California San Diego, Department of Chemistry and Biochemistry Gembicky, Milan; University of California San Diego, Chemistry and Biochemistry Okuno, Saya; University of California San Diego, Chemistry and Biochemistry Chan, Thomas; University of California, San Diego, Department of Nanoengineering; University of California San Diego, Department of Chemistry and Biochemistry Batista, Victor; Yale University, Chemistry

PM-IRRAS and DFT investigation of the surface orientation of new Ir piano-stool complexes attached to Au (111)

Christopher J. Miller,§[a] Felix M. Brunner,§[a] H. Ray Kelly,[b] Po Ling Cheung,[a] Nicole A. Torquato,[a] Milan Gembicky,[a] Saya Okuno,[a] Thomas Chan,[a] Victor S. Batista,[b] Clifford P. Kubiak*[a]

a. Department of Chemistry and Biochemistry, University of California, San Diego, 9500 Gilman Drive, Mail Code 0358, La Jolla, California 92093-0358
b. Department of Chemistry and Energy Sciences Institute, Yale University, 225 Prospect Street, New Haven, Connecticut 06520, United States

§ These authors contributed equally to the work.

*Corresponding Author E-mail: ckubiak@ucsd.edu

Abstract

Surface immobilization of organometallic catalysts is a promising approach to developing new catalytic systems that combine molecular catalysts with heterogenous surfaces to probe surface mechanisms. The orientation of the catalyst relative to the surface is one important parameter that must be considered in such hybrid systems. In this work, we synthesize three new sulfide-modified Ir piano-stool complexes with sulfide-modified bipyridine and phenylpyridine ligands for the attachment to Au (111) surfaces. Self-assembled monolayers made from (Cp*Ir(2,2'-bipyridine-4-sulfide)Cl]$_2$[Cl]$_2$ (**C1m**) and [Cp*Ir(2-phenylpyridine-4-sulfide)Cl]$_2$ (**C2m**) were characterized by combining polarization modulation infrared reflection absorption spectroscopy (PM-IRRAS) with DFT calculations of the minimum energy orientations of the complexes on the surface. We find that the bipyridine and phenylpyridine ligands are oriented at between 73-77° relative to the surface normal, irrespective of the orientation of the other ligands. Additionally, DFT and PM-

IRRAS support the orientation of **C1m** to be a mixed monolayer with a slight preference for the Cl oriented down toward the Au surface and **C2m** to also slightly favor the Cl down orientation.

Introduction

Iridium piano-stool complexes, such as [Ir(Cp*)(bpy)(Cl)]Cl and Ir(Cp*)(ppy)(Cl) (where Cp*=pentamethylcyclopentadienyl, bpy = 2,2'-bipyridine and ppy = 2-phenylpyridine) are highly active catalysts for a wide range of fundamental transformations, including electrochemical and photochemical hydrogen evolution[1-5] and transfer hydrogenation/dehydrogenation of ketones[6-10], olefins[11, 12], formic acid[13, 14], and CO_2.[15-17] These types of catalysts are generally selective, tunable, easy to characterize, and their mechanisms can be well understood via conventional spectroscopies. Heterogeneous catalysts, on the other hand, are often touted for their stability, activity, scalability, low catalyst loadings required on supports, and ease of separation of products. In contrast to homogeneous catalysts, their mechanisms are often more difficult to interpret due to the intrinsic difficulty in analyzing surfaces. This lack of mechanistically informed synthesis often hinders catalyst design, so catalyst discovery often relies on high-throughput screening and predictive modeling as opposed to rational design.[18] Thus, surface immobilization of molecular catalysts aims to provide the benefits of both homogeneous molecular and heterogeneous catalysts.[19]

Previously, iridium piano-stool complexes have been attached to semiconductor surfaces[20-25]; however, their orientation on the surface was not described. The orientation of these catalysts could have significant effects on activity, as the bulky cyclopentadienyl or surface may block substrates from reacting with the Ir center.[24, 26] Au surfaces are ideal for this type of study as surface attachment via self-assembled monolayers of thiols and disulfides is a well-established,

covalent attachment strategy.[27-29] In addition, the properties of Au allow for surface-sensitive IR characterization using polarization modulation infrared reflection absorption spectroscopy (PM-IRRAS).[30-32] PM-IRRAS has already been shown to be a useful tool for determining average binding orientation for organic thiols[33-35], electrochemical absorbates[36-38], and molecular catalysts[27, 39-43] on conducting surfaces. Due to the selection rules of PM-IRRAS on metal surfaces, p-polarized light will interact with the absorbed molecules and only transition dipole moments (TDM) with a component normal to the surface will absorb the light, reinforced by the image dipole.[31, 44-46] The relative absorption of these transition dipole moments, coupled with density functional theory (DFT) calculations are useful in determining the average molecular orientation of SAMs on Au.

Herein, we describe the synthesis and characterization of three new Ir piano-stool complexes with sulfur modified bipyridine and phenylpyridine ligands (**C1**, **C2**, and **C3**). The differences in the reactivities of these ligands and the synthesis of the complexes are described. Self-assembled monolayers of **C1** and **C2** were made and characterized, giving two new surface-immobilized Ir complexes on Au surfaces. Using PM-IRRAS and DFT, the average molecular orientations on the surface were determined.

Results and Discussion

Synthesis and Characterization of Ligands

To prevent direct reactivity of a free thiol with the iridium center, which is known to readily react with thiolate ligands[47], disulfides were chosen over free thiols as the attachment strategy (Fig. 1). Disulfides are also known to cleave upon self-assembly onto Au surfaces without generating byproducts.[29] Both ligands di(2,2'-bipyridine)-4-disulfide (**bpySSbpy**) di(2-phenylpyridine)-4-

disulfide (**ppySSppy**) were synthesized from their corresponding 4-chloro-pyridine derivatives. 4-chloro-2,2'-bipyridine was synthesized using a literature procedure or was obtained from commercial sources.[48]

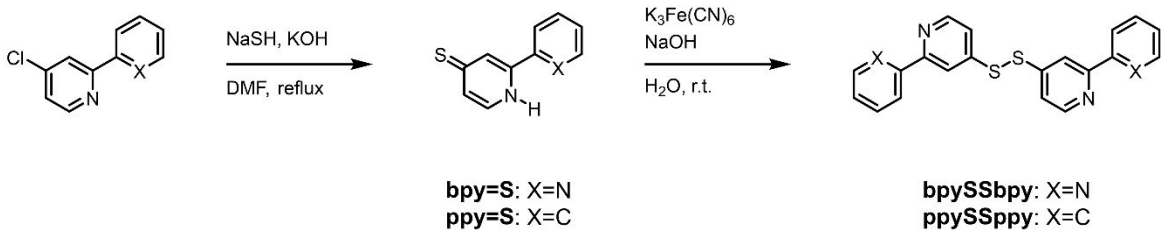

Fig. 1. Synthesis of disulfide ligands bpySSbpy and ppySSppy.

4-chloro-2-phenylpyridine was obtained by cross-coupling of phenylboronic acid with 2-bromo-4-chloropyridine following a literature procedure.[49] The pyridine-chlorides were converted into thiones through nucleophilic aromatic substitution of the chloride with sodium hydrogen sulfide in basic DMF following modified literature procedures.[27, 50] The dry NaSH was replaced with technical grade NaSH · xH_2O with no adverse effects on the reaction. The same procedure was used to synthesize 4-thione-2-phenylpyridine. Both thiones are insoluble in neutral water but readily dissolve under basic conditions. Oxidation of the thiones yields the more stable disulfide. The previously reported procedure used catalytic NaI and hydrogen peroxide as the oxidant which resulted in low yields of under 40%.[27] Since the reaction proceeds through a simple outer sphere electron transfer, any oxidant with a sufficient oxidation potential can be used. The oxidation of the thione to disulfide is best carried out in aqueous conditions. Potassium ferricyanide is a readily available water-soluble oxidant with a sufficient oxidation potential. Furthermore, it is otherwise inert under the reaction conditions, preventing side reactions and the only byproduct is water-soluble ferrocyanide. Upon addition of the oxidant, the disulfide is formed immediately and precipitates out under the reaction conditions, while all other species are highly water-soluble. The

disulfides were isolated in almost quantitative yield by filtration. If pure thione is used in the reaction no further purification steps are necessary. However, we found that purification of **ppySSppy** by flash column chromatography efficiently removes possible impurities from previous steps.

Synthesis and Characterization of Molecular Complexes

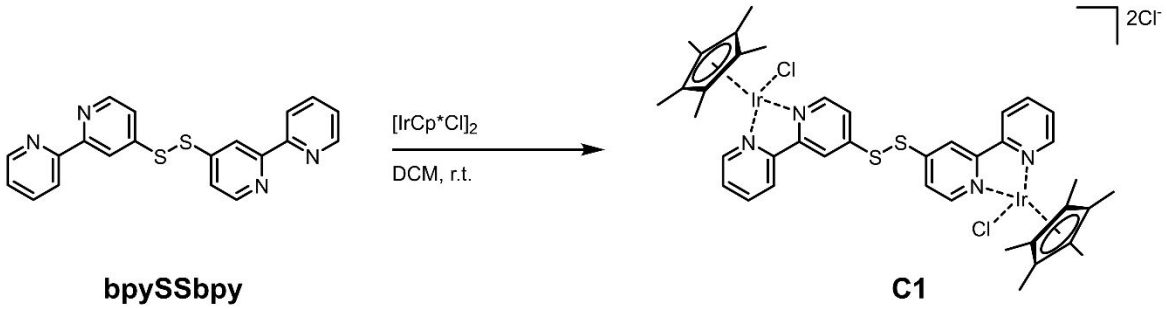

Fig. 2. Synthesis of C1 from the corresponding ligand and $[Ir(Cp^*)Cl_2]_2$ dimer.

$[Cp^*Ir((2,2'\text{-bipyridine-4-sulfide})Cl]_2[Cl]_2$ (C1). Metalation of the bpySSbpy ligand with $[Ir(Cp^*)Cl_2]_2$ led to the formation of $[Cp^*Ir((2,2'\text{-bipyridine-4-sulfide})Cl]_2[Cl]_2$ (C1). The metalation can be carried out in MeOH or DCM under an inert atmosphere. Using MeOH as the solvent had several drawbacks. First, the low solubility of the iridium precursor in MeOH requires the reaction to be carried out at 40 °C. Under these conditions, to avoid the formation of partially metalated ligand, a slight excess of metal was used in this procedure. The reaction mainly yielded the title compound with slight impurities of excess starting material and side products. Purification by flash column chromatography over neutral alumina improved the purity of the product. Carrying out the reaction in DCM (Fig. 2) has several advantages. The higher solubility of the starting material permitted running the reaction at room temperature which led to a cleaner reaction. Furthermore, the elimination of MeOH as a solvent allowed us to carry out the reaction and purification in a glove box, providing rigorous exclusion of oxygen and water and simplifying

handling. This also allowed us to utilize stoichiometric amounts of ligand and metal and resulted in improved purity. In addition, the product is highly hygroscopic, quickly picking up water in air, leading to difficulty in purification. This can be seen in the ATR-IR spectra of the compound taken in air, leading to a broad peak between 3100-3600 cm^{-1} (Fig. S22B). However, this peak did not appear in the ATR-IR of the product when the reaction and ATR-IR measurement was done in the glovebox (Fig. S22A). Precipitation from DCM through the addition of THF resulted in pure product.

The iridium center in **C1** is an enantiomeric center, making molecules of this type chiral. Only few reports mention the chiral nature of the molecules, often when it represents the key component of the work.[51, 52] Utilizing the disulfide dimer **bpySSbpy** as a ligand, we connect the two chiral metal centers from each complex, leading to the formation of diastereomers. While the difference between the diastereomers is not very large, the two diastereomers can be distinguished in proton NMR (Fig. S10 and S11). The Cp* experiences a different environment in both diastereomers, leading to two distinct peaks in the ^{1}H NMR centered at δ=1.71 ppm. The splitting is influenced by the solvent. While in chloroform, there is a measurable separation of 0.02 ppm (Fig. 3) between the two Cp* peaks, in acetonitrile the two peaks almost coalesce with a separation of only 0.0015 ppm (Fig. S10). For the bipyridine there are also distinguished peaks observed for

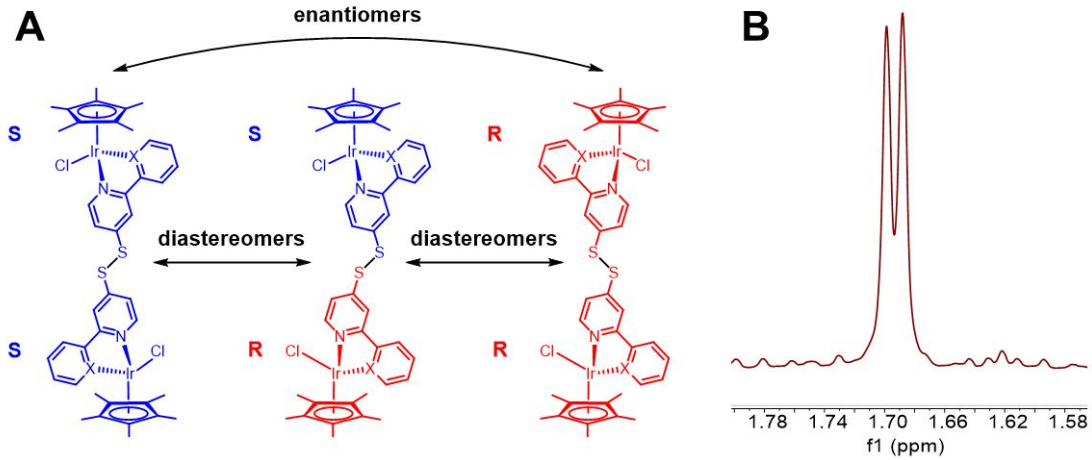

Fig. 3. A) Representation of the enantiomers (S,S and R,R) and diastereomers (S,S and R,R are diastereomer of S,R) of **C1**: X=N or **C2**: X=C that are formed as a statistical mixture. B) the ^{1}H NMR of the methyl protons on the Cp* ring showing the splitting due the chirality at the metal of **C1** in $CDCl_3$.

several protons. This further illustrates the similarity of the two isomers, and the influence the solvent has on the dynamics of the molecule. Attempts to separate the two diastereomers by fractional crystallization were not successful but also unnecessary for further use in surface modification. During the formation of the SAM, the disulfide bond is homolytically cleaved by the Au surface.[27, 29] This cleavage of the disulfide yields monomers that are chiral enantiomers, not diastereomers.

[Cp*Ir(2-phenylpyridine-4-sulfide)Cl]$_2$ (C2) and [Cp*Ir(2-phenylpyridine-4-thiol)]$_3$ (C3). Initial attempts to cyclometalate [Ir(Cp*)Cl$_2$]$_2$ with **ppySSppy** resulted in the formation of a

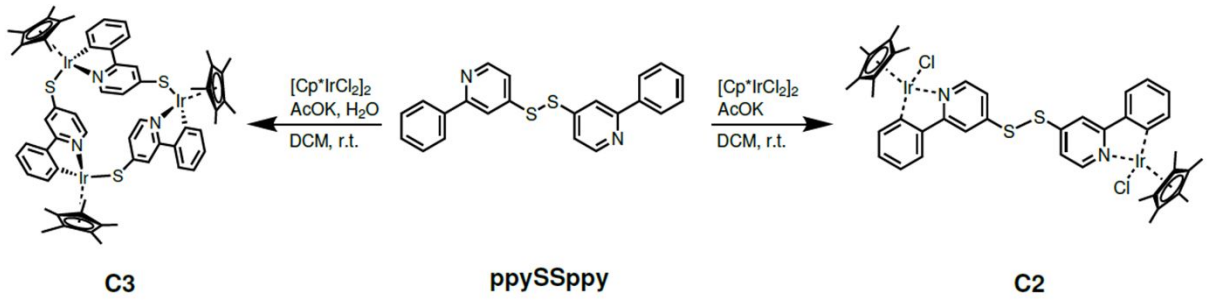

Fig. 4. Synthesis of **C2** from the corresponding ligand and [Ir(Cp*)Cl$_2$]$_2$ dimer (right). The same reaction conditions in the presence of trace water lead to the formation of **C3** (left).

mixture of eight different compounds that could be separated by flash column chromatography. Only the first fraction was identified. An X-ray crystal structure (Fig. S43) was obtained that corresponds to the trimer [Cp*Ir(2-phenylpyridine-4- thiol)]$_3$ (**C3**). The iridium is bonded to one unit of the phenylpyridine and the next unit of thiol. If the reaction is carried out under rigorous exclusion of water and oxygen in a nitrogen-filled glove box, C2 is formed as the predominant product (Fig. 4). We speculate that the formed [Cp*IrppyCl] complex can lose the chloride ligand in the presence of water and cleave the disulfide.[53] We believe that evidence of this is seen in the ATR-IR of **C2** done in air. A weak, broad peak ranging

from 3200-3600 cm^{-1} corresponding to $\nu_{stretch}$(O-H) of water forms once the compound is brought into air (Fig. S23B). We believe this leads to the formation of different oligomers with the **C3** trimer being a particularly stable species that is formed in significant quantities. Similar to **C1**, the $\nu_{stretch}$(O-H) does not appear in the ATR-IR of the purified compound taken in a N_2-filled glovebox. As with the bipyridine counterpart, **C2** is also chiral and isolated as a statistical mixture of enantiomers.

Complex Orientation On Au Surface by DFT Calculations

Table 1. Orientational and energetic parameters of the DFT optimized (wB97XD functional and the DEF2SVP basis set) structures of **C1m** and **C2m** shown in Fig. 5.

Structure	Cl orientation	Tilt angle (°) θ_1	Tilt angle (°) θ_2	Twist Angle (°) ψ_1	Relative Energy (kcal/mol)	S-Au (Å)
C1m	Up	75	23	91	0	2.39
	Down	77	76	268	-2.8	2.47
C2m	Up	73	23	93	-1.8	2.26
	Down	76	74	269	0	2.32

Disulfide bonds are known to cleave in the presence of a gold surface to form self-assembled monolayers. In the case of the **C1** and **C2** dimers, the disulfide bond breaks to form a monolayer of the monomer, herein referred to as **C1m** and **C2m** respectively. Following our previous studies,[26, 27, 54-56] the lowest energy binding modes for **C1m** and **C2m** were determined using DFT. In accordance with experimental measurements discussed later, **C3** was found to have very weak interactions with the Au surface precluding the characterization of a well-defined binding geometry. All calculations were performed in Gaussian 16, Revision C.01[57] using the ωB97X-D functional;[58] nonmetal atoms were treated with a 6-31G(d,p) basis set[59-61] and the DEF2SVP basis

set and pseudopotential[62] were used on Ir and Au (see SI for further discussions about the computational method). Frequency calculations were used to confirm stationary points and perform spectroscopic analysis of **C1m** and **C2m**.

To characterize the binding modes of **C1m** and **C2m** on the surface, we utilize the Euler angles relating to the molecular frame to the laboratory frame fixed on the gold surface according to tilt (θ), twist (ψ), and rotation (phi) (Fig. 5A and B). Here, θ_1 refers to the tilt angle of the

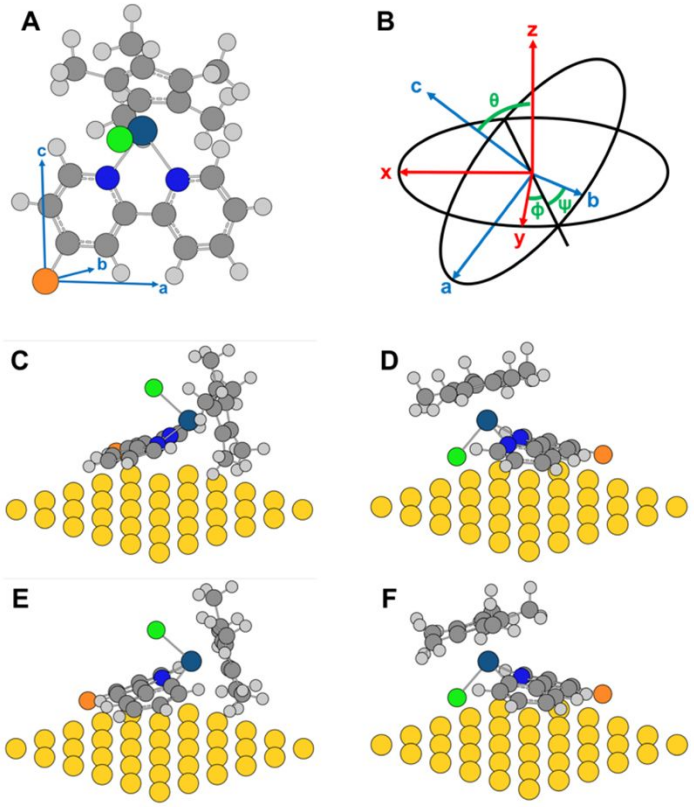

Fig. 5. (A) Definition of axes in molecular frame (a, b, c) using **C1m** as an example. (B) Euler angle definition for a molecular orientation relative to the laboratory frame (x, y, z). DFT optimized structures (wB97XD functional and the DEF2SVP basis set) of **C1m** (C, D) and C2m (E, F) on a Au cluster showing the minimum binding modes of the complexes in the Cl up (C and E) and Cl down (D and F) orientations. Color code for atoms: yellow = Au, orange = S, gray = C, white = H, blue = N, navy = Ir, green = Cl

bipyridine for **C1** and phenylpyridine for **C2** and θ_2 refers to the tilt of the Cp* angle relative to the surface normal. The geometry could not be assumed for monolayers formed for **C1m** and

C2m. Therefore, two possible DFT-optimized geometries were determined for each complex, one with the chloride atom pointing towards the surface (Cl down) and the other pointing away (Cl up). Other considered starting orientations optimized to either the Cl down or Cl up geometry.

The four DFT optimized orientations of **C1m** and **C2m** are depicted in **Fig. 5** and their relevant geometrical parameters and energetics are described in **Table 1**. Interestingly, DFT indicates that the **C1m** and **C2m** have different preferred orientations. For **C1m**, the Cl up orientation is 2.8 kcal/mol higher in energy compared to the Cl down orientation. For **C2m**, the relative energy for the Cl down orientation is 1.8 kcal/mol higher than that of the Cl up orientation. However, in both cases, the small energy differences indicate that there is unlikely to be a preferred orientation of the monolayers formed on the surface experimentally. However, the energy difference does motivate direct comparison with PM-IRRAS to confirm this under experimental conditions.

In both orientations, the θ_1 and ψ_1 of both **C1m** and **C2m** differ by only a few degrees, with the two ranging between 73° and 77° for θ_1 and ψ_1 being slightly off parallel with the surface. The orientation of both the phenylpyridine and bipyridine match previous reports[27, 55] of using similar ligands on Au. In addition, the steric bulk of the Cp* ring does not seem to significantly affect the binding orientation in the Cl up orientation as there is only at most a 3° change in the tilt angle (θ_1) between the two orientations. The similarity in orientation between the two complexes indicates that there is not a significant impact on binding due to overall charge of the complexes.

The DFT can provide insight into future reactivity studies. In both **C1m** and **C2m** in the Cl down orientation, the Cp* ligand to lies above the complex, at 76° and 74° off normal, respectively. This orientation possibly blocks substitution of the chloride ligand, hindering

reactivity. However, in the Cl up orientation for **C1m** and **C2m**, the Cp* ligand lies at 23° off surface normal for both, allowing for substitution and substrate access to the iridium metal center.

Orientation Determination Via PM-IRRAS and DFT

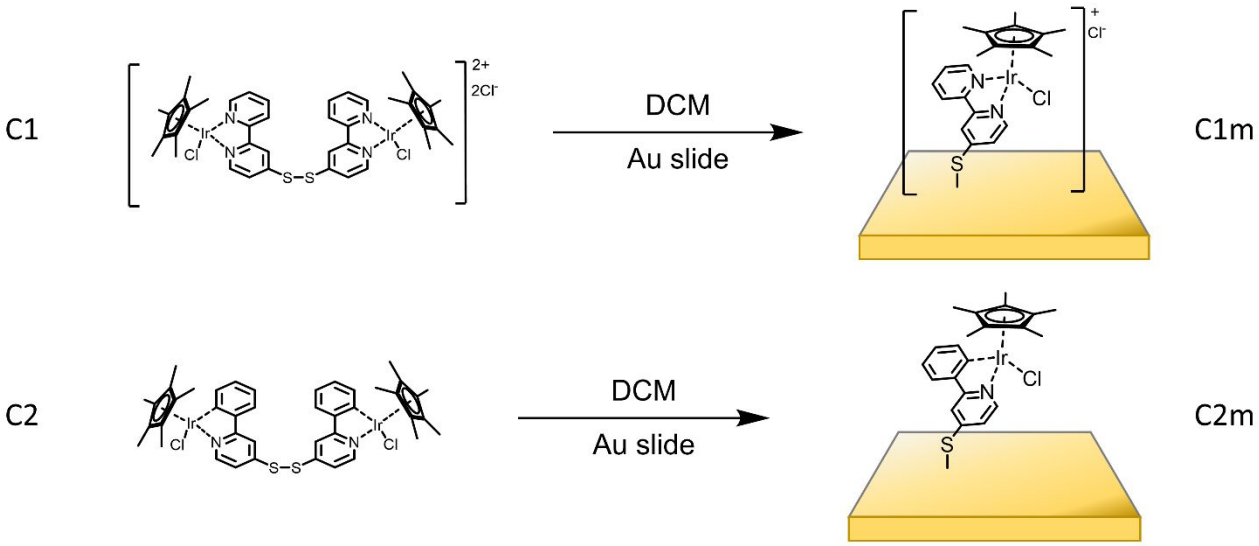

Fig. 6. Representation of the surface modification of Au (111) with complexes **C1** and **C2** to form monolayers **C1m** and **C2m**.

Polarization modulation infrared reflection-absorption spectroscopy (PM-IRRAS) is a useful tool for determination of monolayer orientation. The intensity of PM-IRRAS spectral lines is dependent on the angle of the transition dipole moment of the vibrational modes. For Au surfaces, there is an electric field amplitude normal to the surface. For transition dipole moments with amplitude normal to the surface, there is an enhancement in signal that is proportional to the magnitude of the dipole moment and angle off normal of that transition. As shown in previous studies[63, 64], the anisotropic amplitude enhancement, the integrated absorbance for a transition dipole moment normal to the surface is three times as large as the integrated absorbance of an isotropic arrangement of molecules in a thin film of same thickness (Equation 1).

$$\cos^2\theta = \frac{\int A_{exp}}{3\int A_{sim}} \quad (1)$$

Therefore, a comparison can be made between the isotropic FTIR absorbance of complexes **C1**, and **C2**, in a KBr pellet and the anisotropic PM-IRRA spectra. Determination of the orientation of the monolayers was done by direct comparison of the spectral fits of the PM-IRRAS and the simulated IRRAS from the KBr giving an experimentally determined orientation of the TDM. This value was then compared to the TDMs and relative intensity of the transitions determined from the DFT calculations (See Supporting Information).

To determine which of the calculated orientations exist on the surface, self-assembled monolayers of **C1** and **C2** were made by soaking a clean Au-coated slide in a 1 mM solution of the corresponding complex in dry DCM in a N_2 filled glovebox for 24 h (Fig. 6). The sample was then washed with DCM and dried under N_2 before characterization. C3 was excluded from this analysis as the monolayer did not survive this washing step with DCM prior to analysis. XPS analysis of the monolayers show that the Ir remains in the expected Ir(III) oxidation state along with the corresponding Cl, N, and S peaks that are expected for these complexes (See supporting information). In addition, the narrow line widths of the PM-IRRA spectra and relative agreeance with the molecular spectra indicate an intact monolayer on the surface. Inductively coupled plasma mass spectroscopy (ICP-MS) and X-ray photoelectron spectroscopy (XPS) corroborates this data. ICP-MS determines the surface coverage of **C1m** to be 1.25×10^{-9} mol/cm^2 and **C2m** to be 2.20×10^{-10} mol/cm^2. However, the $\nu_{stretch}$(C-H) frequency was not useful for orientation determination due to the fact that peaks were not above the noise level of the instrument. This result indicates that the dipole moments for these transitions have insignificant amplitude normal to the surface.

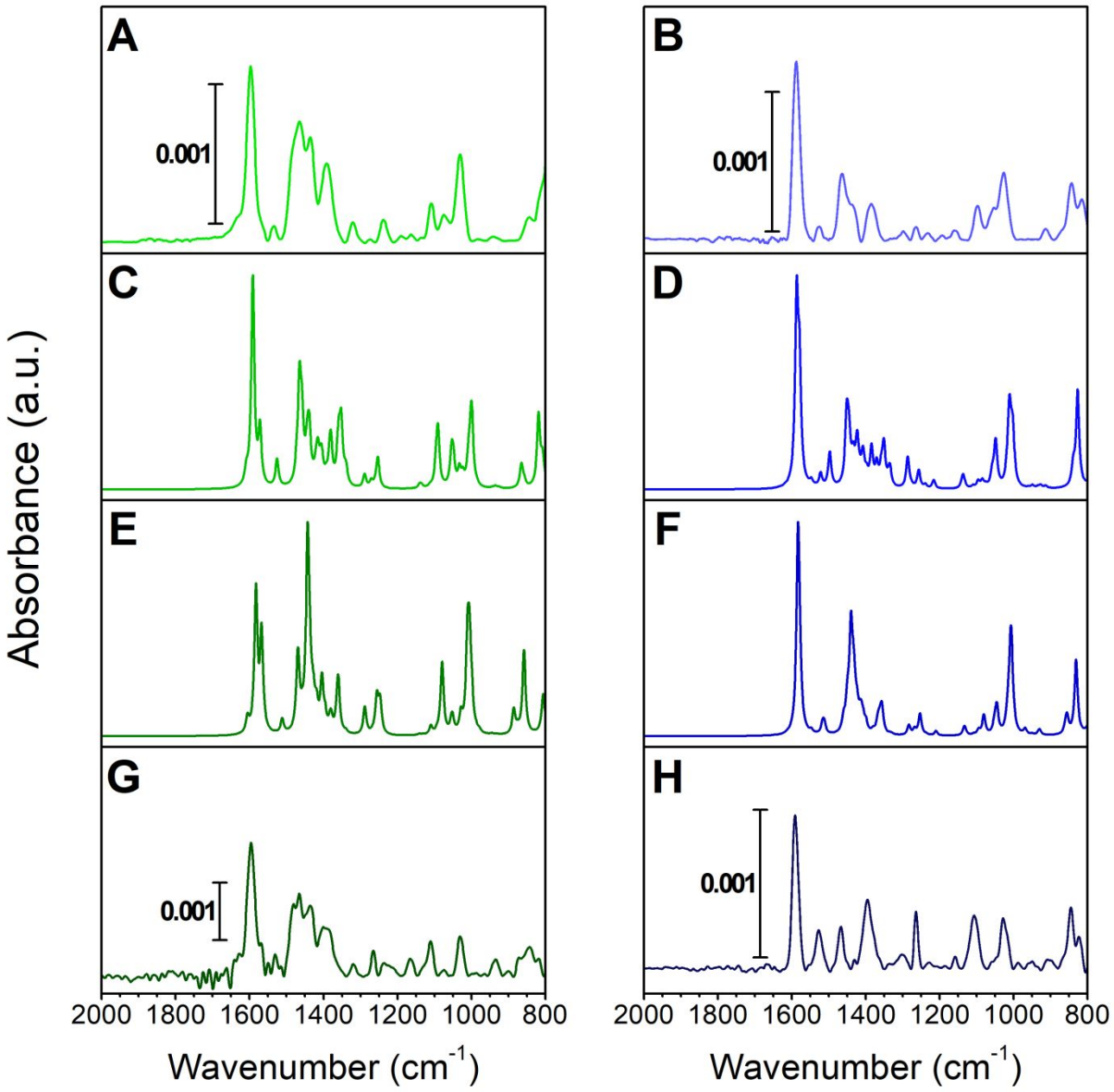

Fig. 7. Experimental and computational spectra of **C1m** (green) and **C2m** (blue) on Au. The isotropic simulated IRRA spectra from the KBr (A and B), DFT (wB97XD functional and the DEF2SVP basis set with a 0.9485 scaling factor) calculated IR spectra in the Cl up orientation (C and D) and Cl down (E and F) and the PM-IRRA spectra of the monolayers adsorbed on Au. (G and H).

For **C1m**, there appears to no preferred orientation of the complex present on the surface. A full analysis of the angles of the TDM with respect to orientation and analysis of the PM-IRRAS, DFT, and simulated isotropic IRRAS data can be found in the supporting information. Briefly, the DFT (wB97XD functional and the DEF2SVP basis set) analysis indicates that, while the relative

intensities of the calculated spectra for the Cl up spectra are a closer approximation of the PM-IRRA spectra, the TDM analysis is inconclusive in determining a preferred orientation. The most intense transition in this region, at 1597 cm^{-1}, arises from the pyridine breathing modes. The experimental orientation of this TDM is determined to be around 40° off normal. DFT indicates that there are four bipyridine breathing modes between 1609 cm^{-1} and 1512 cm^{-1} that differ due to the asymmetry induced by the thiolate in the 4 position of the bipyridine. However, the orientation of the TDM of these transitions are not significantly different for the Cl up and down orientations and range between 16° and 50° off normal with the averages for each orientation being around 26° for the Cl down and about 20° for the Cl up°, showing relative agreement within the possible bounds of the experiment (see Supporting Information). The more indicative peaks for determining the orientation of the compound on the surface are those transitions that are from the Cp* ligand. As stated above, **Table 1** shows the change in tilt angle, θ_2, of the Cp* ligand off surface normal. DFT indicates that this large orientation difference leads to significant differences in the angle of the TDM of the molecular vibrations from the Cp* ligand. The $\nu_{bending}$(C-H) modes of the methyl groups in the Cp* ligand have vibrational transitions between 1480-1420 cm^{-1} and around 1020 cm^{-1} as well as a mix of $\nu_{bending}$(C-H) and $\nu_{breathing}$(C-C) vibrations around 1390 cm^{-1} and 1320 cm^{-1}.[24, 65, 66] However, for the transitions between 1480 cm^{-1} and 1320 cm^{-1}, the angles of the TDM determined from the DFT for these peaks do not differ significantly. The peak that shows the largest difference between the isotropic spectra and the PM-IRRAS is at 1075 cm^{-1}. DFT indicates that this peak corresponds to a mix of asymmetric $\nu_{bending}$(C-H) on the Cp* and bipyridine ligand and breathing modes in the pyridines. While DFT indicates that there is not much difference in the determined angle of the TDM (14° for Cl down and 19° for Cl up), the orientation of the monolayer does lower the energy of this transition in the Cl up orientation by 22 cm^{-1} to 1053 cm^{-1}. Due to

the variance in the angles of the TDM determined experimentally compared to the DFT calculated TDM and considering the small difference in binding energy determined by DFT, it is likely that the monolayers are not uniform, consisting of a mixture of orientations persisting on the surface.

Similar to **C1m**, there appears to be no preferred orientation of **C2m** present on the surface. A full analysis of the angles of the TDM with respect to orientation and analysis of the PM-IRRAS data of **C2** can be found in the supporting information. Briefly, the DFT determined TDM for the transition at 1587 cm^{-1} corresponding to the phenylpyridine breathing mode does not change angle significantly depending on orientation of the complex on the surface being 27° and 37° off normal for Cl down and 31° and 36° off normal for Cl up. However, they do differ significantly from the experimentally determined TDM of 61°. In addition, there are two peaks in the PM-IRRAS that have significantly lower absorbances as compared to the isotropic spectra and DFT computed spectra. First, the transition at 1448 cm^{-1} has a significant decrease in absorbance for the PM-IRRAS spectra, giving a determined TDM angle of 83°. DFT indicates that this band is the combination of transitions primarily of the asymmetric $\nu_{bending}$(C-H) mode of the methyls on the Cp* ligand. The computed TDMs for these transitions for the Cl down orientation are 44°, 32° and 75° off normal and 37°, 50°, and 5° off normal for the Cl up orientation. In addition, the symmetric C-H wagging mode of the methyls on the Cp* ligand at 1058 cm^{-1} also has a significant decrease in absorbance in the PM-IRRAS when compared to the simulated isotropic spectra. The experimentally determined TDM is 78° off normal. The DFT determines that there are two TDMs, 75° and 25° off normal for the Cl down orientation and 23° and 26° for the Cl up orientation. However, these two transitions, along with the discrepancy between the other TDM angles determined experimentally and DFT suggests that there is a mixture of orientations on the surface.

This is further corroborated by the relative binding energy determined by DFT, as the computed difference of 1.8 kcal/mol is small enough that it can be overcome under experimental conditions.

Conclusion

There is a growing interest in understanding the orientation of molecular catalysts immobilized on surfaces to gather insights to the mechanisms that arise in heterogenized catalysis. We reported the synthesis and characterization of three new Cp*Ir piano-stool complexes, [Cp*Ir((2,2'-bipyridine-4-sulfide)Cl]$_2$[Cl]$_2$ (**C1**), [Cp*Ir(2-phenylpyridine-4-sulfide)Cl]$_2$ (**C2**), and [Cp*Ir(2-phenylpyridine-4-thiol)]$_3$ (**C3**). By combining DFT and PM-IRRAS, we have investigated the average orientation for the monolayers of **C1m** and **C2m** formed on Au(111). The relative agreement of the experimental data with both orientations as well as the small difference in binding energy determined by DFT suggests that there is likely a mixed orientation **C1** monolayer. Similarly, the PM-IRRAS and DFT calculated spectra for **C2m** suggests that there is a no preference for the Cl down or Cl up orientation, with a mixture of orientations present on the surface. These conclusions show the strength in combining DFT and PM-IRRAS in the determination of orientation of organometallic compounds on Au surfaces even in the absence of a strong IR absorber. In addition, the mixed orientation of these compounds can provide insights into future reactivity studies in substituting the chloride motif with other substrates.

Experimental Section

General Methods and Materials

^{1}H were recorded on a Bruker 300 MHz or JOEL 500 MHz spectrometer. ^{13}C NMR spectra were recorded on a JEOL 500 MHz spectrometer. The ^{13}C and ^{1}H Chemical shifts are referenced to deuterated solvent peaks and reported relative to TMS ($\delta = 0$). ATR-FT-IR spectra were recorded on a Bruker Alpha II. Transmission spectra of KBr pellets of **C1, C2**, and **C3** were acquired on a

Thermo Scientific Nicolet 6700. A detailed description of the determination of the simulated IRRAS spectra from these KBr pellets can be found in the SI. Acquired spectra were averaged over 32 scans at a 4 cm^{-1} resolution. Mass spectrometry was performed on a Micromass Quattro Ultima. High resolution Mass spectrometry was performed on an Agilent 6230 Accurate-Mass TOFMS. XPS was performed on an SSF-Kratos AXIS-SUPRA. Mass spectrometry was performed on a Micromass Quattro Ultima. Solvents were received from Fisher Scientific and were dried on a custom solvent system (degassed with Argon and dried over alumina columns) and stored over 3 Å sieves. Deuterated solvents were obtained from Cambridge Isotope Laboratories. Flash column chromatography was performed on a Teledyneisco CombiFlash Rf200 using SiO_2 or neutral alumina loaded columns. 2,2'-bipyridine-N-oxide,[48] 4-chloro-2,2'-bipyridine,[48] 4-thione-2,2'-bipyridine,[27] and di(2,2'-bipyridine)-4-disulfide,[27] $[Ir(Cp^*)Cl_2]_2$[67] were synthesized following previously reported procedures. All other reagents were obtained from commercial sources and used without further purification. Where stated, reactions under nitrogen atmosphere were performed using standard Schlenk-line and Glove Box techniques.

Synthesis of 4-thione-2,2'-bipyridine (bpy=S)

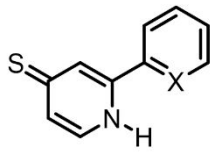

The compound was synthesized using a modified literature procedure[50], $NaSH \cdot xH_2O$ (16.80 g, 70 %, 209.83 mmol, 20.0 eq.) was added to DMF (100 mL) and the mixture was deoxygenated by sparging with N_2. To it, 4-chloro-2,2'-bipyridine (2.0 g, 10.49 mmol, 1.0 eq.) and KOH (1.77 g, 31.47 mmol, 3.0 eq.) were added and the mixture was deoxygenated by sparging with N_2 again.

The mixture was heated to light reflux for 24 h (high reflux rates led to sublimation and subsequent deposition of NaSH in the condenser). After cooling to room temperature (if not cooled to room temperature prior to air exposure a brown precipitate forms that complicates workup and adversely effects the yield) the solution was filtered to remove the white precipitate, rinsed with ethyl acetate and the was solvent was removed from the combined filtrate under reduced pressure. The residue was dissolved in H_2O (50 mL) and the pH was set to neutral with aqueous HCl (2M). The solution was extracted with DCM (3 x 50 mL) and the combined organic layers were washed with brine (50 mL) and dried over $MgSO_4$. The solvent was removed under vacuum and the residue crystallized from EtOH to yield the title compound as a crystalline orange/yellow solid (1.44 g, 7.65 mmol, 73%) Proton NMR matches reference.[50]

^{1}H NMR (300 MHz, CD3CN) δ/ppm 11.34 (bs, 1H), 8.73 - 8.68 (m, 1H), 8.09 (d, J = 8.1 Hz, 1H), 8.00 - 7.91 (m, 2H), 7.56 - 7.47 (m, 2H), 7.31 (dd, J = 6.7, 2.0 Hz, 1H).

Synthesis of di(2,2'-bipyridine)-4-disulfide (bpySSbpy)

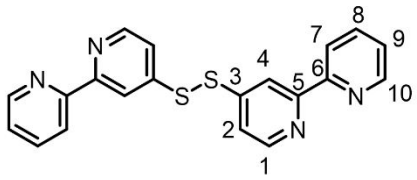

In air, 4-thione-2,2'-bipyridine (1.00 g, 5.31 mmol, 1.0 eq.) was solubilized in H_2O (100 mL) by addition of NaOH (233.72 mg, 5.84 mmol, 1.1 eq.). At room temperature a solution of potassium ferricyanide (1.92 g, 5.84 mmol, 1.1 eq.) in H_2O (20 mL) was added. A white precipitate was formed immediately, and the mixture was stirred for 2 h. The precipitate was filtered off and washed thoroughly with water. After drying under vacuum the title compound was obtained as a white solid (949 mg, 2.53 mmol, 95%). Proton and carbon NMR matches reference.[27]

^{1}H NMR (500 MHz, $CDCl_3$) δ /ppm 8.67 (ddd, J = 4.8, 1.7, 0.9 Hz, 1H, H^{10}), 8.61 - 8.51 (m, 2H, $H^{4,1}$), 8.37 (dt, J = 7.9, 1.0 Hz, 1H, H^{7}), 7.81 (td, J = 7.8, 1.8 Hz, 1H, H^{8}), 7.44 (dd, J = 5.3, 2.0 Hz, 1H, H^{2}), 7.32 (ddd, J = 7.5, 4.8, 1.2 Hz, 1H, H^{9}).

^{13}C{^{1}H} NMR (126 MHz, $CDCl_3$) δ /ppm 156.5 (C^{5}), 155.4 (C^{6}), 149.6 (C^{1}), 149.4 (C^{10}), 148.1 (C^{3}), 137.2 (C^{8}), 124.3 (C^{9}), 121.6 (C^{7}), 119.8 (C^{2}), 117.9 (C^{4}).

IR (ATR) ν_{max} [cm^{-1}]: 3079 (w), 3057 (w), 1573(s), 1561(s), 1537(s), 1447(s), 1377(s), 1271(m), 996(m), 829(m), 790(s), 745(m), 702(s), 657(m), 619(m), 593(m).

Synthesis of 4-thione-2-phenylpyridine (ppy=S)

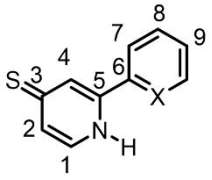

4-chloro-2-phenylpyridine (800 mg, 4.22 mmol, 1.0 eq.), NaSH x H_2O (6.76 g, 70 %, 84.37 mmol, 20.0 eq.), and KOH (710.04 mg, 12.66 mmol, 3.0 eq.) were added to DMF (50 mL) and the mixture was deoxygenated by sparging with N_2 (g). The mixture was heated to light reflux for 24 h (high reflux rates lead to sublimation and subsequent deposition of NaSH in the condenser). After cooling to room temperature (if not cooled to room temperature prior to air exposure a brown precipitate forms that complicates workup and adversely effects the yield) the solution was filtered and washed with ethyl acetate and the solvent was removed under reduces pressure. The residue was dissolved in H_2O (50 mL) and pH was set to neutral with aqueous HCl (2M). The precipitate was filtered off and washed with water. After drying under vacuum the title compound was obtained as a yellow solid (Yield: 663 mg, 3.54 mmol, 84%).

^{1}H NMR (300 MHz, $(CD_3)_2SO$) δ/ppm 12.76 (s, 1H, H^{N-H}), 7.78 - 7.73 (m, 2H, H^{7}), 7.62 (d, J = 6.7 Hz, 1H, H^{1}), 7.58 - 7.55 (m, 3H, $H^{8, 9}$), 7.47 (d, J = 1.9 Hz, 1H, H^{4}), 7.18 (dd, J = 6.7, 2.0 Hz, 1H, H^{2}).

^{1}H NMR (300 MHz, $CDCl_3$) δ/ppm 7.70-7.63 (m, 3H, $H^{1, 7}$), 7.57 (d, J = 1.9 Hz, 1H, H^{4}), 7.45-7.39 (m, 3H, $H^{8, 9}$), 7.20 (dd, J = 6.3, 1.9 Hz, 1H, H^{2}).

^{13}C{^{1}H} NMR (126 MHz, $(CD_3)_2SO$) δ/ppm 190.60 (s, C3), 143.37 (s, C^{5}), 133.66 (s, C1), 132.48 (s, C^{6}), 130.65 (s, C^{9}), 129.26 (s, C^{8}), 128.57 (s, C2), 127.36 (s, C^{4}), 127.07 (s, C^{7}).

IR (ATR) ν_{max} [cm^{-1}]: 3300 (b), 3063 (b), 2942 (b), 1606 (s), 1575 (s), 1499 (w), 1471 (m), 1454 (m), 1409 (m), 1301 (m), 1230 (w), 1096 (s), 989 (w), 900 (w), 814 (s), 766 (s),713 (m), 692 (s), 626 (w), 609 (w), 522 (m).

HR-ESI-MS: m/z calcd for $[M]^+$ 188.0527 (found) 188.052; calcd for $[M + H]^+$ 187.0450 (found) 187.0450.

EA: Anal. Calcd for $C_{11}H_9NS$: C, 70.55%; H, 4.8%;N 7.5%; 17.1%. Found: C, 70.2 %; H, 4.9%; N, 7.6%; S 17.5%.

Synthesis of di(2-phenylpyridine)-4-disulfide

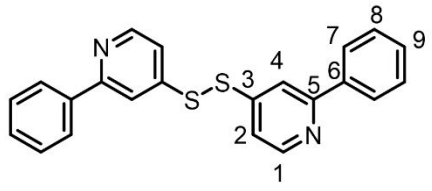

In air, 4-thione-2-phenylpyridine(500 mg, 2.67 mmol, 1.0 eq.) was partially solubilized in H_2O (50 mL) by addition of NaOH (117 mg, 2.94 mmol 1.1 eq.). At room temperature a solution of potassium ferricyanide (967 mg, 2.94 mmol, 1.1 eq.) in H_2O (20 mL) was added. A white precipitate was formed immediately, and the mixture was stirred for 1 day. The solid was filtered

off over Celite® and washed thoroughly with water. The residue was redissolved in DCM, filtered and the solvent was removed under reduced pressure. The residue was purified by flash column chromatography (SiO2, DCM). The first peak corresponded to the title compound and was isolated as an off-white solid (Yield: 433 mg, 1.16 mmol, 87 %).

^{1}H NMR (500 MHz, $CDCl_3$) δ/ppm 8.59 (dd, J = 5.3, 0.6 Hz, 2H, H1), 7.95 - 7.92 (m, 4H, H^7), 7.82 (dd, J = 1.8, 0.6 Hz, 2H, H^4), 7.48 - 7.41 (m, 6H, $H^{8,9}$), 7.35 (dd, J = 5.3, 1.9 Hz, 2H, H^2).

^{13}C{^{1}H} NMR (126 MHz, $CDCl_3$) δ/ppm 158.2 (C^5), 150.0 (C^1), 147.5 (C^3), 138.7 (C^6), 129.6 (C^8), 129.0 (C^9), 127.2 (C^7), 118.5 (C^2), 117.0 (C^4).

IR (ATR) ν_{max} [cm^{-1}]: 3032 (m), 2916 (m), 2848 (m), 1564 (s), 1538 (s), 1459 (m), 1438 (m), 1372 (m), 1069 (w), 1052 (w), 824 (m), 793 (w), 769 (s), 725 (m), 685 (s), 632 (m), 590 (m).

HR-ESI-MS: m/z calcd for [M + H]+ 373.0828 (found) 373.0828.

EA: Anal. Calcd. for $C_{22}H_{16}N_2S_2$: C, 70.9%; H, 4.3%; 7.5%; 17.2%. Found: C, 70.6 %; H, 4.7%; N, 7.55%; S 16.9%.

Synthesis of (Cp*Ir(2,2'-bipyridine-4-sulfide)Cl]$_2$[Cl]$_2$ (C1)

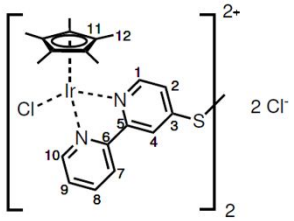

To a solution of $[Cp^*IrCl_2]_2$ (150 mg, 188.28 μmol, 1.0 eq.) in dry DCM (15 mL) in the glovebox, bpySSbpy (70.51 mg, 188.28 μmol, 1.0 eq.) was added. The solution was stirred at room temperature for 1 day. The solvent was removed under vacuum and the resulting yellow solid was

purified by precipitation from DCM through the addition of THF. The solid was filtered off and dried under vacuum to yield the title compound as a bright yellow solid (Yield: 197 mg, 164.0 μmol, 87%). The product was isolated as a statistical mixture of diastereomers. Numbers annotated with (') in the NMR data refer to signals corresponding to different diastereomers. The complex is air-stable but highly hygroscopic and was stored and handled in a nitrogen filled glove box.

^{1}H NMR (500 MHz, MeCN) δ/ppm 9.36 (s, 2H, $H^{4/4'}$), 9.32 (s, 2H, $H^{4'/4'}$), 9.17 (d, J = 8.1 Hz, 2H, $H^{7/7'}$), 9.13 (d, J = 8.1 Hz, 2H, $H^{7/7'}$), 8.87 (dd, J = 5.6, 1.1 Hz, 4H, $H^{10,\ 10'}$), 8.81 (d, J = 6.2 Hz, 2H, $H^{1/1'}$), 8.78 (d, J = 6.2 Hz, 2H, $H^{1/1'}$), 8.20 (t, J = 7.9 Hz, 4H, $H^{8,\ 8'}$), 8.07 (dd, J = 6.2, 2.0 Hz, 2H, $H^{2/2'}$), 8.00 (dd, J = 6.2, 2.0 Hz, 2H, $H^{2/2'}$), 7.81 - 7.74 (m, 4H, $H^{9,\ 9'}$), 1.64 - 1.60 (m, J = 1.2 Hz, 60H, $H^{12,\ 12'}$).

^{13}C{^{1}H} NMR (126 MHz, MeCN) δ/ppm 156.26 (s, $C^{5/5'}$), 156.21 (s, $C^{5/5'}$), 155.63 (s, $C^{6,\ 6'}$), 152.72 (s, $C^{10,\ 10'}$), 152.67 (s, $C^{3/3'}$), 152.64 (s, $C^{3/3'}$), 152.43 (s, $C^{1/1'}$), 152.29 (s, $C^{1/1'}$), 141.24 (s, $C^{8/8'}$), 141.22 (s, $C^{8/8'}$), 130.09 (s, $C^{9,\ 9'}$), 126.33 (s, $C^{2/2'}$), 126.30 (s, $C^{7/7'}$), 126.28 (s, $C^{7/7'}$), 125.97 (s, $C^{2/2'}$), 122.93 (s, $C^{4/4'}$), 122.82 (s, $C^{4/4'}$), 90.42 (s, C^{11}), 8.78 (s, C^{12}).

IR (ATR) ν_{max} [cm^{-1}]: 3059 (w), 2972 (m), 2916 (w), 2873 (w), 1595 (s), 1537 (w), 1463 (m), 1431 (m), 1390 (m), 1322 (w), 1238 (w), 1110 (m), 1063 (w), 1031 (m), 849 (w), 812 (w), 790 (s), 754 (w), 715 (w), 594 (m).

HR-ESI-MS: m/z calcd. for [M - 2Cl]2+ 550.0804 (found) 550.0807 (isotope pattern matches simulated spectrum, Fig. S31).

EA: Anal. Calcd. For $C_{40}H_{44}Cl_4Ir_2N_4S_2$ x $5H_2O$: C, 38.09%; H, 4.32%; N, 4.44%; S, 5.08%. Found: C, 38.10%; H, 4.31%; N, 4.52%; S, 5.13%.

Synthesis of [Cp*Ir(2-phenylpyridine-4-sulfide)Cl]$_2$ (C2)

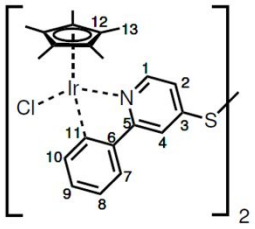

$[Cp^*IrCl_2]_2$ (213.88 mg, 268.45 μmol, 1.0 eq.), di(2-phenylpyridine)-4-disulfide (100.00 mg, 268.45 μmol, 1.0 eq.) and potassium acetate (158.08 mg, 1.61 mmol, 6.0 eq.) were mixed in dry DCM and stirred at room temperature for 22 h in a glovebox under N_2. The reaction mixture was filtered over Celite® and the solvent was removed from the filtrate. The orange residue was purified by flash column chromatography (SiO2, DCM to DCM/10% MeOH). The solvent was removed under vacuum to yield the title compound as a bright orange solid (189 mg, 172.4 μmol, 64%). The product was isolated as a statistical mixture of diastereomers. Numbers annotated with (') in the NMR data refer to signals corresponding to different diastereomers.

^{1}H NMR (500 MHz, CDCl3) δ/ppm 8.57 - 8.56 (m, 2H, $H^{1, 1'}$), 7.91 - 7.87 (m, 2H, $H^{4, 4'}$), 7.83-7.79 (m, 2H, $H^{10, 10'}$), 7.68 -7.62 (m, 2H, $H^{7, 7'}$), 7.24 - 7.15 (m, 4H, $H^{9, 9', 2, 2'}$), 7.06 - 6.99 (m, 2H, $H^{8, 8'}$), 1.69 - 1.64 (m, 30H, $H^{13, 13'}$).

^{13}C{^{1}H} NMR (126 MHz, CDCl3) δ/ppm 167.52 ($C^{5/5'}$), 167.36 ($C^{5/5'}$), 164.38 ($C^{11/11'}$), 164.34 ($C^{11/11'}$), 151.40 ($C^{1/1'}$), 151.23 ($C^{1/1'}$), 147.93 ($C^{3/3'}$), 147.84 ($C^{3/3'}$), 143.17 ($C^{6/6'}$), 143.09 ($C^{6/6'}$), 136.07 ($C^{10,10'}$), 131.70 ($C^{9/9'}$), 131.68 ($C^{9/9'}$), 124.30 ($C^{7,7'}$), 122.37 ($C^{8/8'}$), 122.32 ($C^{8/8'}$), 118.73 ($C^{2/2'}$), 118.49 ($C^{2/2'}$), 115.40 ($C^{4/4'}$), 115.07 ($C^{4/4'}$), 88.90 ($C^{12,12'}$), 9.10 ($C^{13,13'}$).

IR (ATR) ν_{max} [cm^{-1}]: 2956 (m), 2920 (s), 2851 (s), 1721 (w), 1686 (w), 1587 (s), 1460 (s), 1378 (m), 1261 (m), 1090 (m), 1026 (m), 822 (m), 806 (m), 772 (m), 729 (s).

HR-ESI-MS: m/z calcd. for [M - 2Cl]2+ 512.1085 (found) 512.1090 isotope pattern matches simulated spectrum (SI Fig. S32).

EA: Anal. Calcd. For $C_{42}H_{44}Cl_2Ir_2N_2S_2$: C, 46.0%; H, 4.05%; N, 2.6%; S, 5.85%. Found: C, 46.1%; H, 4.3%; N, 2.4%; S, 5.5%.

Synthesis of [Cp*Ir(2-phenylpyridine-4-thiol)]$_3$ (C3)

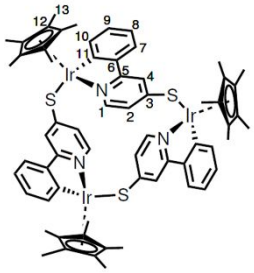

To degassed DCM (10 mL) in a Schlenk flask [Cp · $IrCl_2]_2$ (176.45 mg, 221.47 μmol, 1.1 eq.), 1,2-bis(2-phenylpyridin-4-yl)disulfide (75 mg, 201.34 μmol, 1.0 eq.), potassium acetate (118.56 mg, 1.21 mmol, 6.0 eq.) were added, resulting in an orange solution with a white precipitate. The mixture was stirred at room temperature for 1 day. The solid was filtered off and the solvent was removed from the filtrate under vacuum. The resulting orange residue was purified by flash column chromatography (SiO2, DCM to DCM/5% MeOH). The first peak was isolated as a bright yellow/orange solid (40 mg, 26.01 μmol, 19 %). Crystals suitable for X-ray diffraction were grown by slow evaporation of pentane into a solution of the complex in 1,2-dichlorobenzene.

^{1}H NMR (500 MHz, $CDCl_3$) δ/ppm 8.01 (d, J = 6.3 Hz, 3H, H^1), 7.44 (d, J = 1.9 Hz, 3H, H^4), 7.42 (d, J = 7.6 Hz, 3H, H^{10}), 7.29 (dd, J = 7.8, 0.9 Hz, 3H, H^7), 7.07 (td, J = 7.5, 1.3 Hz, 3H, H^9), 6.89 (td, J = 7.7, 1.1 Hz, 3H, H^8), 6.74 (dd, J = 6.3, 2.0 Hz, 3H, H^2), 1.80 (s, 45H, H^{13}).

$^{13}C\{^{1}H\}$ NMR (126 MHz, $CDCl_3$) δ/ppm 163.33 (s, C^3), 162.30 (s, C^{11}), 158.53 (s, C^5), 148.02 (s, C^1), 144.44 (s, C^6), 134.29 (s, C^{10}), 130.16 (s, C^9), 123.62 (s, C^7), 123.26 (s, C^2), 122.03 (s, C^8), 121.31 (s, C^4), 89.97 (s, C^{12}), 9.06 (s, C^{13}).

IR (ATR) ν_{max} [cm^{-1}]: 3045 (w), 2916 (w), 2851 (w), 1738 (w), 1589 (s), 1507 (w), 1466 (m), 1444 (m), 1381 (m), 1292 (w), 1263 (w), 1235 (w), 1156 (w), 1106 (m), 1098 (m), 1016 (m), 859 (w), 819 (m), 770 (m), 725 (s), 714 (w), 663 (w), 638 (w), 611 (w), 537 (w).

HR-ESI-MS: m/z calcd. for $[M + H]^+$ 1538.3329 (found) 1538.3357 (isotope pattern matches a $[M]^+$ / $[M+H]^+$ ratio of 0.58 / 0.42, Fig. S33).

EA: Anal. Calcd. For $C_{63}H_{66}Ir_3N_3S_3$: C, 49.2%; H, 4.3%; N, 2.7%; S, 6.25%. Found: C, 49.4%; H, 4.6%; N, 3.0%; S, 6.5%.

Preparation of Au and self-assembled monolayers

All samples for PM-IRRAS, ICP-MS, and XPS were prepared on optically flat Au substrates consisting of a layer of Cr (1-4 nm) and Au (200-300 nm) evaporated onto borosilicate glass slides. The substrates were cleaned by dipping in piranha solution (3:1 H_2SO_4:30% H_2O_2) for 1-2 minutes. ***Caution, piranha solutions are extremely energetic and may result in explosions if not handled with extreme caution.*** The slides were then washed with water and dried. Prior to use, slides were flame treated to remove surface water and then added to 1 mM solutions of the compound in dichloromethane overnight. The slides were then washed with dichloromethane and dried under a stream of nitrogen before analysis.

Polarization Modulation Infrared Reflection-Absorption Spectroscopy (PM-IRRAS)

PM-IRRAS spectra were obtained on a Bruker 55 FTIR with a Bruker PMA 37 accessory under a dry air atmosphere using a Parker Balston Purge Gas Generator. Polarization was achieved using

a PEM-90-D ZnSe Photoelestic Modulator (Hinds Instruments) operating at 50 kHz and half-wave retardation coupled with a Synchronous Sampling Demodulator (GWC Instruments). A liquid nitrogen cooled mercury cadmium telluride detector equipped with a BaF_2 window detector was used and set at an angle of incidence of 88˚ with respect to normal. Scans were collected for 2000 scans each sum and difference with 4 cm^{-1} resolution and maximum dephasing at either 1600 cm^{-1} and 3000 cm^{-1} to minimize PM error across the entire spectra. Baseline was established by previous literature precedent by normalization to a reference (blank) slide.[31, 68, 69] Blank slides were made via the same cleaning method as the samples and allowed to soak in dichloromethane for the same amount of time as the samples. Once baseline corrected, the PM-IRRAS spectra was converted to absorbance values by $A = 0.0223\left[\left(\frac{\Delta I}{I}\right)_{norm} - 1\right]$ where $[\Delta I/I]_{norm}$ is the baseline corrected PM-IRRAS signal.[31] Detailed experimental methods for the fitting of the PM-IRRA spectra for the orientation determination can be found in the SI.

Single Crystal X-ray Diffraction

Single crystal X-ray data was collected on a Bruker Apex II-Ultra CCD diffractometer equipped with MoKα radiation (λ = 0.71073 Å). The crystals were mounted on a Cryo-loop with Paratone oil. Data were collected under a nitrogen gas stream at 100 K using ω and φ scans. Data were integrated using the Bruker SAINT software program and scaled using the SADABS software program. All structures were solved via direct methods with SHELXS[70] and refined by full-matrix least squares procedures using SHELXL21 within the Olex2 small- molecule solution, refinement, and analysis software package.[71] All nonhydrogen atoms were refined anisotropically by full-matrix least-squares (SHELXL-2014). Crystallographic data, structure refinement parameters, and additional notes on structure refinement are summarized in the Supporting Information.

Author Contributions

Synthesis and characterization of complexes: CJM, FMB, PLC, SO. Crystallography: NAT, MG. PM-IRRAS, FTIR, and IRRAS: CJM, TC, SO. ICP-MS: TC. Density Functional Theory: HRK. Analysis: CJM, FMB, HRK. Writing: CJM, FMB, HRK, VB, CPK. Editing of manuscript: All. Supervision: VB, CPK.

Conflicts of interest

There are no conflicts to declare.

Acknowledgements

We acknowledge Joseph Palasz, Sarah Tyler, Dr. Michael Neville, and Prof. Tianquan (Tim) Lian for invaluable discussions and the UCSD Molecular Mass Spectrometry Facility for HRMS sample analysis. This work was supported by the Air Force Office of Scientific Research under Award No. FA9550-17-0198. The authors acknowledge Dr. Ich Tran and the use of facilities and instrumentation at the UC Irvine Materials Research Institute (IMRI), which is supported in part by the National Science Foundation through the UC Irvine Materials Research Science and Engineering Center (DMR-2011967). XPS was performed using instrumentation funded in part by the National Science Foundation Major Research Instrumentation Program under grant no. CHE-1338173.

REFERENCES

1. S. M. Barrett, B. M. Stratakes, M. B. Chambers, D. A. Kurtz, C. L. Pitman, J. L. Dempsey and A. J. M. Miller, *Chem. Sci.*, 2020, **11**, 6442-6449.
2. C. L. Pitman and A. J. M. Miller, *ACS Catal.*, 2014, **4**, 2727-2733.
3. B. M. Stratakes and A. J. M. Miller, *ACS Catal.*, 2020, **10**, 9006-9018.

4. K. R. Brereton, A. G. Bonn and A. J. M. Miller, *ACS Energy Lett.*, 2018, **3**, 1128-1136.
5. S. M. Barrett, S. A. Slattery and A. J. M. Miller, *ACS Catal.*, 2015, **5**, 6320-6327.
6. S. Ogo, N. Makihara, Y. Kaneko and Y. Watanabe, *Organometallics*, 2001, **20**, 4903.
7. T. Abura, S. Ogo, Y. Watanabe and S. Fukuzumi, *J. Am. Chem. Soc.*, 2003, **125**, 4149.
8. A. H. Ngo, M. Ibanez and L. H. Do, *ACS Catal.*, 2016, **6**, 2637-2641.
9. T. P. Brewster, A. J. M. Miller, D. M. Heinekey and K. I. Goldberg, *J. Am. Chem. Soc.*, 2013, **135**, 16022-16025.
10. R. Kawahara, K.-i. Fujita and R. Yamaguchi, *J. Am. Chem. Soc.*, 2012, **134**, 3643-3646.
11. Y. Himeda, N. Onozawa-Komatsuzaki, S. Miyazawa, H. Sugihara, T. Hirose and K. Kasuga, *Chem. Eur. J.*, 2008, **14**, 11076.
12. J.-t. Liu, S. Yang, W. Tang, Z. Yang and J. Xu, *Green Chem.*, 2018, **20**, 2118-2124.
13. A. F. Sasayama, C. E. Moore and C. P. Kubiak, *Dalton Trans.*, 2016, **45**, 2436-2439.
14. N. Onishi, M. Iguchi, X. Yang, R. Kanega, H. Kawanami, Q. Xu and Y. Himeda, *Adv. Energy Mater.*, 2019, **9**, 1801275.
15. Y. Himeda, N. Onozawa-Komatsuzaki, H. Sugihara and K. Kasuga, *Organometallics*, 2007, **26**, 702-712.
16. S. Sanz, M. Benítez and E. Peris, *Organometallics*, 2010, **29**, 275.
17. S. Ogo, R. Kabe, H. Hayashi, R. Harada and S. Fukuzumi, *Dalton Trans.*, 2006, 4657-4663.
18. L. An and R. Chen, *J. Power Sources*, 2016, **320**, 127-139.
19. R. M. Bullock, A. K. Das and A. M. Appel, *Chem. Eur. J.*, 2017, **23**, 7626-7641.
20. P. K. Poddutoori, J. M. Thomsen, R. L. Milot, S. W. Sheehan, C. F. A. Negre, V. K. R. Garapati, C. A. Schmuttenmaer, V. S. Batista, G. W. Brudvig and A. van der Est, *J. Mater. Chem. A*, 2015, **3**, 3868-3879.
21. G. F. Moore, J. D. Blakemore, R. L. Milot, J. F. Hull, H.-e. Song, L. Cai, C. A. Schmuttenmaer, R. H. Crabtree and G. W. Brudvig, *Energy Environ. Sci.*, 2011, **4**, 2389-2392.
22. K. S. Joya, N. K. Subbaiyan, F. D'Souza and H. J. M. de Groot, *Angew. Chem. Int. Ed.*, 2012, **51**, 9601-9605.
23. H. Tong, Y. Jiang, Q. Zhang, J. Li, W. Jiang, D. Zhang, N. Li and L. Xia, *ChemSusChem*, 2017, **10**, 3268-3275.
24. K. L. Materna, B. Rudshteyn, B. J. Brennan, M. H. Kane, A. J. Bloomfield, D. L. Huang, D. Y. Shopov, V. S. Batista, R. H. Crabtree and G. W. Brudvig, *ACS Catal.*, 2016, **6**, 5371-5377.

25. J. R. C. Lattimer, J. D. Blakemore, W. Sattler, S. Gul, R. Chatterjee, V. K. Yachandra, J. Yano, B. S. Brunschwig, N. S. Lewis and H. B. Gray, *Dalton Trans.*, 2014, **43**, 15004-15012.
26. A. Ge, B. Rudshteyn, P. E. Videla, C. J. Miller, C. P. Kubiak, V. S. Batista and T. Lian, *Acc. Chem. Res.*, 2019, **52**, 1289-1300.
27. M. L. Clark, A. Ge, P. E. Videla, B. Rudshteyn, C. J. Miller, J. Song, V. S. Batista, T. Lian and C. P. Kubiak, *J. Am. Chem. Soc.*, 2018.
28. C. E. D. Chidsey and D. N. Loiacono, *Langmuir*, 1990, **6**, 682-691.
29. A. Ulman, *Chem. Rev.*, 1996, **96**, 1533-1554.
30. W. G. Golden, D. S. Dunn and J. Overend, *J. Catal.*, 1981, **71**, 395-404.
31. T. Buffeteau, B. Desbat and J. M. Turlet, *Appl. Spectrosc.*, 1991, **45**, 380-389.
32. E. A. Monyoncho, V. Zamlynny, T. K. Woo and E. A. Baranova, *Analyst*, 2018, **143**, 2563-2573.
33. V. Lebec, J. Landoulsi, S. Boujday, C. Poleunis, C. M. Pradier and A. Delcorte, *J. Phys. Chem. C*, 2013, **117**, 11569-11577.
34. C. Silien, M. Buck, G. Goretzki, D. Lahaye, N. R. Champness, T. Weidner and M. Zharnikov, *Langmuir*, 2009, **25**, 959-967.
35. W. Luo, S. M. Legge, J. Luo, F. Lagugné-Labarthet and M. S. Workentin, *Langmuir*, 2020, **36**, 1014-1022.
36. X. Bin, I. Zawisza, J. D. Goddard and J. Lipkowski, *Langmuir*, 2005, **21**, 330-347.
37. L. Kékedy-Nagy, E. E. Ferapontova and I. Brand, *J. Phys. Chem. B*, 2017, **121**, 1552-1565.
38. V. Zamlynny, I. Zawisza and J. Lipkowski, *Langmuir*, 2003, **19**, 132-145.
39. J. Wang, M. L. Clark, Y. Li, C. L. Kaslan, C. P. Kubiak and W. Xiong, *J. Phys. Chem. Lett.*, 2015, **6**, 4204-4209.
40. F. Petersen, I. Lautenschläger, A. Schlimm, B. M. Flöser, H. Jacob, R. Amirbeigiarab, T. R. Rusch, T. Strunskus, O. Magnussen and F. Tuczek, *Dalton Trans.*, 2021, **50**, 1042-1052.
41. A. Schlimm, N. Stucke, B. M. Flöser, T. Rusch, J. Krahmer, C. Näther, T. Strunskus, O. M. Magnussen and F. Tuczek, *Chem. Eur. J.*, 2018, **24**, 10732-10744.
42. H. Jacob, K. Kathirvel, F. Petersen, T. Strunskus, A. Bannwarth, S. Meyer and F. Tuczek, *Langmuir*, 2013, **29**, 8534-8543.
43. N. M. Orchanian, L. E. Hong, J. A. Skrainka, J. A. Esterhuizen, D. A. Popov and S. C. Marinescu, *ACS Appl. Energy Mater.*, 2019, **2**, 110-123.
44. D. L. Allara and R. G. Nuzzo, *Langmuir*, 1985, **1**, 45-52.
45. D. L. Allara and R. G. Nuzzo, *Langmuir*, 1985, **1**, 52-66.

46. M. Gliboff, L. Sang, K. M. Knesting, M. C. Schalnat, A. Mudalige, E. L. Ratcliff, H. Li, A. K. Sigdel, A. J. Giordano, J. J. Berry, D. Nordlund, G. T. Seidler, J.-L. Brédas, S. R. Marder, J. E. Pemberton and D. S. Ginger, *Langmuir*, 2013, **29**, 2166-2174.

47. Y.-K. Sau, X.-Y. Yi, K.-W. Chan, C.-S. Lai, I. D. Williams and W.-H. Leung, *J. Organomet. Chem.*, 2010, **695**, 1399-1404.

48. F. Wang and A. W. Schwabacher, *Tetrahedron Lett.*, 1999, **40**, 4779-4782.

49. F. Brunner, N. Marinakis, C. Wobill, M. Willgert, C. D. Ertl, T. Kosmalski, M. Neuburger, B. Bozic-Weber, T. Glatzel, E. C. Constable and C. E. Housecroft, *J. Mater. Chem. C*, 2016, **4**, 9823-9833.

50. Q. Wang, P. Day, J.-P. Griffiths, H. Nie and J. D. Wallis, *New J. Chem.*, 2006, **30**, 1790-1800.

51. E. B. Bauer, *Chem. Soc. Rev.*, 2012, **41**, 3153-3167.

52. D. Carmona, F. J. Lahoz, R. Atencio, L. A. Oro, M. P. Lamata, F. Viguri, E. San José, C. Vega, J. Reyes, F. Joó and Á. Kathó, *Chem. Eur. J.*, 1999, **5**, 1544-1564.

53. Y.-K. Sau, X.-Y. Yi, K.-W. Chan, C.-S. Lai, I. D. Williams and W.-H. Leung, *J. Organomet. Chem.*, 2010, **695**, 1399-1404.

54. D. Bhattacharyya, P. E. Videla, M. Cattaneo, V. S. Batista, T. Lian and C. P. Kubiak, *Chem. Sci.*, 2021, **12**, 10131-10149.

55. M. L. Clark, B. Rudshteyn, A. Ge, S. A. Chabolla, C. W. Machan, B. T. Psciuk, J. Song, G. Canzi, T. Lian, V. S. Batista and C. P. Kubiak, *J. Phys. Chem. C*, 2016, **120**, 1657-1665.

56. M. Cattaneo, F. Guo, H. R. Kelly, P. E. Videla, L. Kiefer, S. Gebre, A. Ge, Q. Liu, S. Wu, T. Lian and V. S. Batista, *Frontiers in Chemistry*, 2020, **8**.

57. M. J. Frisch, G. W. Trucks, H. B. Schlegel, G. E. Scuseria, M. A. Robb, J. R. Cheeseman, G. Scalmani, V. Barone, G. A. Petersson, H. Nakatsuji, X. Li, M. Caricato, A. V. Marenich, J. Bloino, B. G. Janesko, R. Gomperts, B. Mennucci, H. P. Hratchian, J. V. Ortiz, A. F. Izmaylov, J. L. Sonnenberg, Williams, F. Ding, F. Lipparini, F. Egidi, J. Goings, B. Peng, A. Petrone, T. Henderson, D. Ranasinghe, V. G. Zakrzewski, J. Gao, N. Rega, G. Zheng, W. Liang, M. Hada, M. Ehara, K. Toyota, R. Fukuda, J. Hasegawa, M. Ishida, T. Nakajima, Y. Honda, O. Kitao, H. Nakai, T. Vreven, K. Throssell, J. A. Montgomery Jr., J. E. Peralta, F. Ogliaro, M. J. Bearpark, J. J. Heyd, E. N. Brothers, K. N. Kudin, V. N. Staroverov, T. A. Keith, R. Kobayashi, J. Normand, K. Raghavachari, A. P. Rendell, J. C. Burant, S. S. Iyengar, J. Tomasi, M. Cossi, J. M. Millam, M. Klene, C. Adamo, R. Cammi, J. W. Ochterski, R. L. Martin, K. Morokuma, O. Farkas, J. B. Foresman and D. J. Fox, *Journal*, 2016.

58. J.-D. Chai and M. Head-Gordon, *PCCP*, 2008, **10**, 6615-6620.

59. W. J. Hehre, R. Ditchfield and J. A. Pople, *J. Chem. Phys.*, 1972, **56**, 2257-2261.

60. P. C. Hariharan and J. A. Pople, *Theor. Chim. Acta*, 1973, **28**, 213-222.

61. M. M. Francl, W. J. Pietro, W. J. Hehre, J. S. Binkley, M. S. Gordon, D. J. DeFrees and J. A. Pople, *J. Chem. Phys.*, 1982, **77**, 3654-3665.

62. F. Weigend, *PCCP*, 2006, **8**, 1057-1065.

63. W. N. Hansen, *Journal of the Optical Society of America*, 1968, **58**, 380-390.

64. J. D. E. McIntyre and D. E. Aspnes, *Surf. Sci.*, 1971, **24**, 417-434.

65. H.-D. Amberger and H. Reddmann, *J. Organomet. Chem.*, 2010, **695**, 2455-2460.

66. É. Bencze, B. V. Lokshin, J. Mink, W. A. Herrmann and F. E. Kühn, *J. Organomet. Chem.*, 2001, **627**, 55-66.

67. P. S. Nejman, B. Morton-Fernandez, D. J. Moulding, K. S. Athukorala Arachchige, D. B. Cordes, A. M. Z. Slawin, P. Kilian and J. D. Woollins, *Dalton Trans.*, 2015, **44**, 16758-16766.

68. B. J. Barner, M. J. Green, E. I. Saez and R. M. Corn, *Anal. Chem.*, 1991, **63**, 55-60.

69. T. Buffeteau, B. Desbat, D. Blaudez and J. M. Turlet, *Appl. Spectrosc.*, 2000, **54**, 1646-1650.

70. G. Sheldrick, *Acta Cryst. A*, 2008, **64**, 112-122.

71. O. V. Dolomanov, L. J. Bourhis, R. J. Gildea, J. A. K. Howard and H. Puschmann, *J. Appl. Crystallogr.*, 2009, **42**, 339-341.